LETTER

doi:10.1038/nature12378

Three-state mechanism couples ligand and temperature sensing in riboswitches

Anke Reining[1], Senada Nozinovic[1], Kai Schlepckow[1], Florian Buhr[1], Boris Fürtig[1] & Harald Schwalbe[1]

Riboswitches are *cis*-acting gene-regulatory RNA elements that can function at the level of transcription, translation and RNA cleavage[1–3]. The commonly accepted molecular mechanism for riboswitch function proposes a ligand-dependent conformational switch between two mutually exclusive states[4]. According to this mechanism, ligand binding to an aptamer domain induces an allosteric conformational switch of an expression platform, leading to activation or repression of ligand-related gene expression[5]. However, many riboswitch properties cannot be explained by a pure two-state mechanism. Here we show that the regulation mechanism of the adenine-sensing riboswitch, encoded by the *add* gene on chromosome II of the human Gram-negative pathogenic bacterium *Vibrio vulnificus*[6], is notably different from a two-state switch mechanism in that it involves three distinct stable conformations. We characterized the temperature and Mg^{2+} dependence of the population ratios of the three conformations and the kinetics of their interconversion at nucleotide resolution. The observed temperature dependence of a pre-equilibrium involving two structurally distinct ligand-free conformations of the *add* riboswitch conferred efficient regulation over a physiologically relevant temperature range. Such robust switching is a key requirement for gene regulation in bacteria that have to adapt to environments with varying temperatures. The translational adenine-sensing riboswitch represents the first example, to our knowledge, of a temperature-compensated regulatory RNA element.

The *add* gene contains a structured 112-nucleotide long sequence (Supplementary Fig. 1) within the 119-nucleotide long 5′-untranslated region (5′-UTR) that acts as an adenine-sensing, translational on-riboswitch. Previous studies have focused on the investigation of adenine aptamer domains alone[6–11], and the detailed molecular mechanisms of the conformational switch of full-length riboswitches have remained elusive. The commonly accepted model proposes a ligand-induced switch between two conformations. In any two-state mechanism, complex formation is inherently favoured at low temperatures. Investigating a full-length translational riboswitch[12–14], we found a novel riboswitch mechanism involving three conformations. Efficient switching is maintained over a large temperature range, which is important as the pathogen has to replicate both at 37 °C in the human host and at temperatures around 10 °C in its marine habitat.

In the presence of equimolar amounts of adenine, the ligand-bound holo conformation showed unique tertiary interactions (Fig. 1a and Supplementary Figs 2 and 3). The mode of molecular recognition determined previously for the adenine-bound aptamer domain[15–17] was retained in the full-length riboswitch, as evidenced by the unique pattern of six characteristic NMR imino signals in the binding pocket (Fig. 1b). The three helices P1, P2 and P3 were fully formed and adopted a three-way junction stabilized by long-range interactions between loops L2 and L3. Stabilization of P1 by adenine leads to an opening of P4. Consequently, nucleotides from A111 to U125 were single-stranded, making the Shine–Dalgarno sequence and the AUG start codon accessible to ribosome binding (Fig. 1 and Supplementary Table 1), in line with the biologically observed activation of gene expression of adenosine deaminase in the presence of adenine[12]. This holo conformation of the riboswitch represented the adenine-induced on-state.

Unexpectedly, two ligand-free (apo) conformations instead of one could be detected by NMR. The apoA and apoB conformations revealed markedly different secondary structures (Fig. 1a, Supplementary Fig. 3 and Supplementary Table 2). ApoA was similar to the holo conformation except for the ligand-binding core, the loop–loop interactions and P4. In contrast to previously proposed secondary structure models[12–14,18], P1 and P4 were formed, but only partially. Owing to simultaneous partial formation of both helices, only the Shine–Dalgarno, but not the AUG start codon, was masked in the apoA off-state (Fig. 1a).

The apoB conformation differed considerably from both apoA and holo conformations. The main difference was found in the 5′ region, in which nucleotides in P1 and P2 formed an alternative secondary structure, a helix–bulge–helix (5 base pairs (bp)–7 nucleotides–2 bp) motif capped by a loop of nine nucleotides. P3, P4 and P5 were present, and formation of the ligand-binding three-way junction was suppressed. Structurally, apoB is binding-incompetent; addition of threefold excess of ligand to the riboswitch did not induce any chemical shift perturbations for apoB.

The three conformations were connected by two equilibria: the binding-competent conformation apoA exchanged with the binding-incompetent conformation apoB (equilibrium ratio between the apo states (K_{pre}) = [apoA]/[apoB]), as monitored by NMR exchange spectroscopy[19]. In an adenine-dependent step, apoA could further switch to the holo conformation (dissociation constant (K_d)) (Fig. 1a). The two equilibria were differentially modulated by changes in temperature and Mg^{2+} concentration. K_{pre} changed the population of apoA from 12% to 40% between 10 °C and 30 °C (Fig. 1c). This population ratio was not markedly influenced by Mg^{2+} concentration from 0 to 12 mM ([RNA] = 0.4 mM). By contrast, the binding equilibrium was not only temperature dependent, but also Mg^{2+} dependent. Mg^{2+} stabilized the holo conformation at all temperatures. For example, the addition of 12 mM Mg^{2+} increased the population of holo at 10 °C from 41% to 80%, and at 30 °C from 8% to 76% (Fig. 1c). The stabilizing effect of Mg^{2+} was also reflected in K_d values at different [Mg^{2+}]:[RNA] ratios measured by isothermal titration calorimetry (ITC) (Fig. 1d, e), stopped-flow fluorescence, and NMR (Fig. 2). At 10 °C, the K_d decreased by four orders of magnitude after changing the [Mg^{2+}]:[RNA] ratio from 0 to 2,000:1 (Supplementary Fig. 10). The temperature influence was most prominent at the highest [Mg^{2+}]:[RNA] ratios, for which the K_d increased 100-fold for $\Delta T = 20$ °C.

The rates of interconversion between apoA and apoB were $k_{AB} = 0.91\ s^{-1}$ and $k_{BA} = 0.40\ s^{-1}$ at 25 °C (Fig. 1e and Supplementary Fig. 6a, b). In line with RNA transition-state stabilization, increasing the Mg^{2+} concentrations accelerated these rates (Supplementary Fig. 6c), whereas the populations remained largely unaffected. The 5′-terminal first 35 nucleotides of the riboswitch were responsible

[1]Center for Biomolecular Magnetic Resonance, Institute of Organic Chemistry and Chemical Biology, Johann Wolfgang Goethe-Universität Frankfurt am Main, Max-von-Laue-Strasse 7, 60438 Frankfurt am Main, Germany.

©2013 Macmillan Publishers Limited. All rights reserved

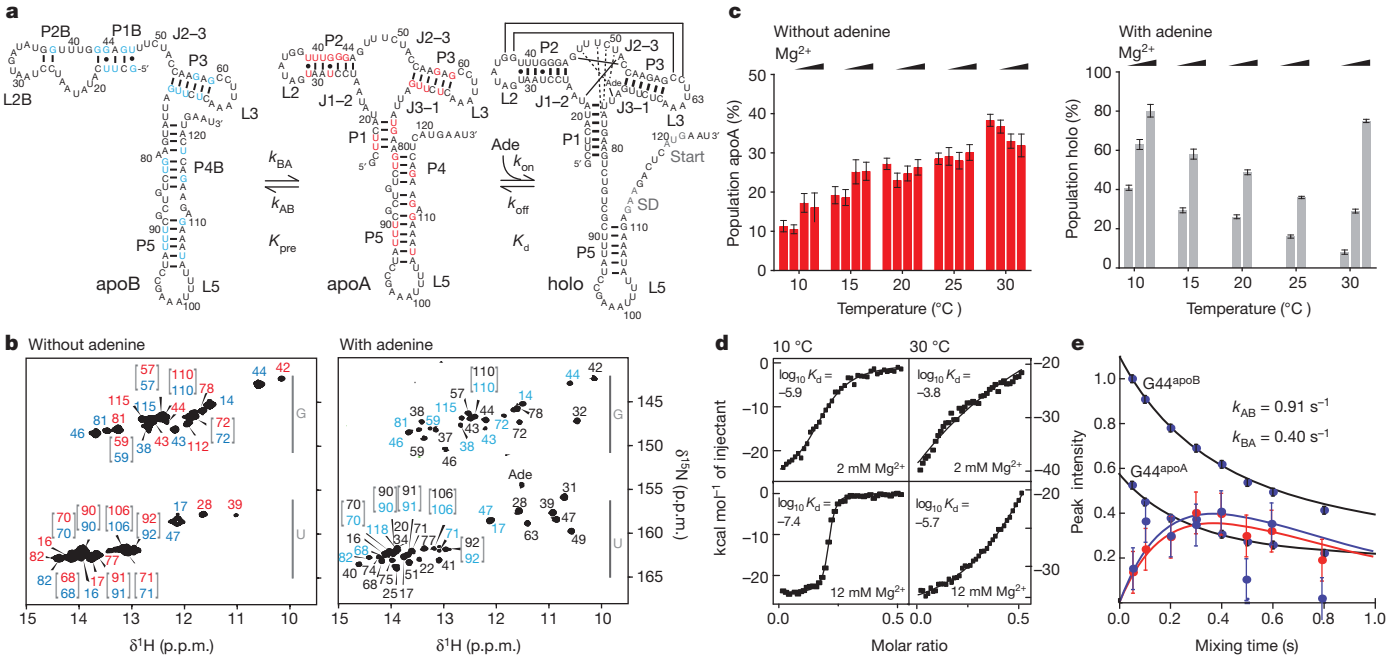

Figure 1 | Modulation of the conformational equilibrium of the wild-type adenine-sensing riboswitch by temperature, Mg^{2+} and cognate ligand. **a**, Secondary structure models of the RNA conformations apoA (assigned nucleotides are red), apoB (blue) and holo (black). The constants (K_{pre} and K_d) and the rates describing the kinetics of interconversion between the conformations in the two equlibria (k_{AB}, k_{BA}, k_{on} and k_{off}) are depicted. **b**, $^{1}H–^{15}N$ HSQC (heteronuclear single quantum coherence) spectra of the imino group region reporting on the base-pairing pattern of each nucleotide of the wild-type RNA (0.6 mM), Mg^{2+} (5 mM), without adenine (left) and with 1.1 eq adenine (right) recorded at 10 °C and 950 MHz. Assigned peaks are annotated for apoA (red), apoB (blue) and holo (black). Conformation apoA was less than 10% populated in the spectrum with adenine and not visible at the given plot level (Supplementary Fig. 5). **c**, Temperature and Mg^{2+} dependence of the populations of the three wild-type RNA conformations in the absence (left) and presence (right) of adenine, obtained by integrated signals ($G115^{apoA}$, $G44^{apoB}$, $U47^{holo}$) in $^{1}H–^{15}N$ HSQC spectra. Populations of [apoA] = 1 − [apoB] (%), and of [holo] = 1 − [apoA + apoB] (%), are shown. Errors were calculated from signal-to-noise (*S*/*N*) ratios of the NMR signals; identical results were obtained for two independent temperature and titration series at 800 MHz and 900 MHz. Mg^{2+} concentrations without adenine are 0, 2, 5 and 12 mM, and with adenine are 0, 5 and 12 mM (only for 10 °C and 30 °C). K_{pre} could be measured with NMR up to 30 °C only, as hydrogen exchange became too rapid at higher temperatures. **d**, Binding of adenine to wild-type monitored by ITC. The curves for binding of wild-type full-length RNA to adenine were recorded at 10 °C and 30 °C with 2 mM and 12 mM Mg^{2+}. Calculated log K_d is given for each binding curve. **e**, Conformational exchange in the apo state monitored by $^{15}N_{ZZ}$-chemical exchange spectroscopy for the wild-type RNA at 25 °C without Mg^{2+}. Black curves describe the decay of the diagonal peaks $G44^{apoA}$ and $G44^{apoB}$ with the mixing time. Blue and red curves describe the build-up and decay of the cross peaks between $G44^{apoA}$ and $G44^{apoB}$. Cross peak intensities are scaled by a factor of 5 in the figure. Errors were calculated from *S*/*N* ratios of the NMR signals used in the analysis, exchange experiments were measured as duplicates and with three different relaxation delays ranging from 2 to 5 s, yielding identical results.

for the conformational heterogeneity in the apo state. This finding was corroborated by analysis of a 35-nucleotide RNA fragment (G14-U49) that showed the same conformational heterogeneity with identical base pairing in the two underlying secondary structure elements (Supplementary Fig. 7). The recently proposed tuning capability of the P2 region in purine-sensing aptamers is in line with the intrinsic bistable character of the first 35 nucleotides described here[20].

To suppress the conformational pre-equilibrium caused by the bistable character and to stabilize the binding-competent conformation apoA, we mutated residues within P2 (Mut^{P2}) (Fig. 2a). The exchange of two AU to GC base pairs (A29C-U41G and A30G-U40C) in P2 (Fig. 2a) led to a thermal stabilization of $\Delta\Delta G = 0.11$ kcal mol^{-1} at 25 °C (Supplementary Fig. 8). In the ligand-free state of Mut^{P2}, a single homogenous set of NMR signals could be detected (Fig. 2b). P2, P3 and P5 were fully formed, as in the holo conformation of the wild-type sequence (Fig. 2b). In addition, P1 and the interaction between L2 and L3 were already pre-formed in Mut^{P2} and the 3′ terminal nucleotides were accessible. No signals reporting the presence of an apoB-like conformation could be detected.

We compared kinetics and thermodynamics of ligand binding to wild-type and Mut^{P2} to determine the effect of the pre-equilibrium at [Mg^{2+}]:[RNA] > 50:1. Binding of the fluorescent adenine analogue 2-aminopurine was characterized by stopped-flow fluorescence spectroscopy (Fig. 2c, d, Supplementary Fig. 10 and Supplementary Tables 3 and 4), as previously conducted[7]. For Mut^{P2}, the K_d values were significantly lower (by a factor of 30 at 10 °C) than the apparent K_d values for the wild type. This discrepancy between the wild-type and Mut^{P2} data can, however, be reconciled if the absolute RNA concentration is corrected for the concentration of the binding-incompetent apoB conformation (Supplementary Fig. 10). Then, ligand affinity to either $apoA^{WT}$ or Mut^{P2} differed only by a factor of 3, strongly suggesting that the pre-equilibrium accounts for it. Tertiary complex formation was characterized by time-resolved NMR[21,22]. For Mut^{P2}, we found the folding rate constant $(k_F) = (10.0 \pm 0.9) \times 10^{-2}$ s^{-1} compared to the wild-type $k_F = (4.0 \pm 0.1) \times 10^{-2}$ s^{-1} (Fig. 2e).

We further examined the functional differences for wild-type and Mut^{P2} in a transcription–translation-coupled luciferase assay (Fig. 3). Analysis of the normalized expression levels showed that Mut^{P2} was not able to control gene expression in an adenine-dependent manner but represented a constitutive on-state. By contrast, the wild type was able to increase expression levels in response to adenine addition. Comparison of the absolute expression levels of the wild type also revealed that the fourfold increase of gene expression over the entire temperature range correlated with a twofold lower overall expression level (Fig. 3).

For a two-state riboswitch, the temperature dependence of K_d makes regulation temperature-dependent for a given ratio of [ligand]:[riboswitch]. Our data for the *add* riboswitch from *V. vulnificus* strongly suggested that its regulation involves three distinct stable conformations. What additional function is conferred to the riboswitch by the

©2013 Macmillan Publishers Limited. All rights reserved

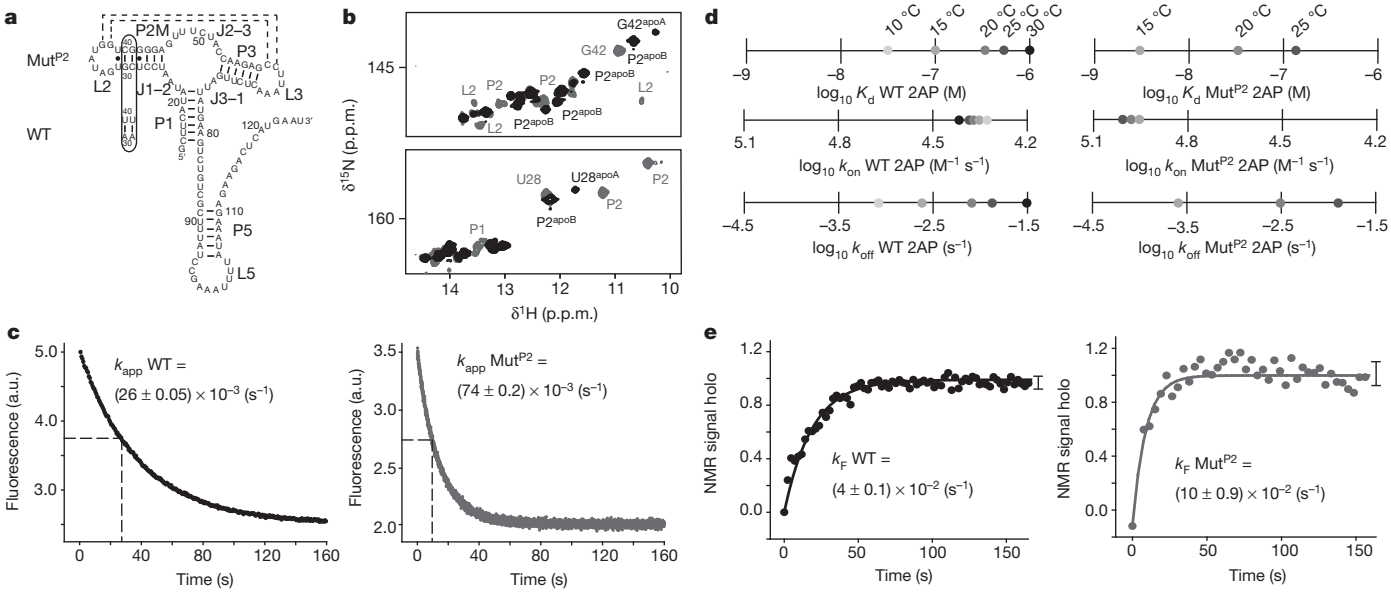

Figure 2 | Comparison of ligand binding kinetics of WT and Mut^{P2} adenine-sensing riboswitch constructs. **a**, Secondary structure of Mut^{P2} RNA in its apo conformation without adenine. Mutation site (A29C-U41G and A30G-U40C) is highlighted in comparison to the wild-type (WT) RNA construct. All detected secondary structure elements are shown. **b**, ^{1}H–^{15}N HSQC spectra indicate the structural differences in the apo states for wild type (black) and Mut^{P2} (grey) in the absence of adenine and Mg^{2+} (20 °C, 900 MHz). Signals arising from conformation apoB are only visible for the wild type. The differences in the overlaid spectra are caused by the mutations in P2. New signals arising from G41 and G30 are visible, whereas those from U40 and U41 are absent. Signals next to the mutation site (U31/U39 and U28/G42) are shifted. Notably different to the wild-type spectra, reporter signals are observable for the loop–loop interactions, indicating the formation of a compact and preformed conformation. **c**, Fluorescence quenching of 2-aminopurine reports on the ligand binding to the adenine-sensing riboswitch. Normalized stopped-flow traces show ligand binding for wild-type (black) and Mut^{P2} (grey), 800 nM RNA, 2 mM Mg^{2+}, 20 °C. Apparent rate constants k_{app} revealed faster binding kinetics for Mut^{P2} than for wild type. Shown are original curves, for the calculation of binding parameters, as depicted in **d** and tabulated in Supplementary Tables 3 and 4. These experiments were independently repeated at least three times, the errors given for the apparent rates are standard errors representing the deviation of the fit from the experimental values. **d**, Stopped-flow binding kinetics, plots of log K_d, log k_{on} and log k_{off} values of wild-type and Mut^{P2} RNA for five and three different temperatures, respectively. The K_d shows a more pronounced temperature dependence for Mut^{P2}. Although k_{on} is only marginally temperature-dependent for both wild type and Mut^{P2}, k_{on} of Mut^{P2} is one order of magnitude larger than k_{on} of the wild type. By contrast, the k_{off} values have a higher temperature dependence but are similar for wild type and Mut^{P2}. The size of error bars, calculated from the mean deviation of triplicate measurements, is smaller than the size of the marks. **e**, Monitoring formation of the holo conformation after ligand binding by real-time NMR. Sum of normalized integrals of imino proton signals from the holo conformation (U31, U39, U47, U49) as a function of time after rapid mixing of the RNA (0.3 mM, 2 mM Mg^{2+}) with adenine (0.6 mM, 2 mM Mg^{2+}) at 20 °C. The displayed error bars were calculated from *S*/*N* ratios of the peaks in the NMR spectra; the wild-type and MutP2 experiments were performed as quadruplicates and duplicates, respectively. Data were fitted mono-exponentially to calculate an apparent rate constant for the formation of the holo conformation k_F. The errors given for the folding rates are standard errors representing the deviation of the fit from the experimental values. Similar to the binding kinetics, complex tertiary structure formation is faster for Mut^{P2} than for the wild type.

pre-equilibrium, with the potential consequence that the cell retains a constitutively inactive fraction of the *add* messenger RNA[23]?

To address this question, we simulated the temperature-dependent change in conformational switching at cellular RNA concentrations of 1 nM[24], according to equation (2) (see Methods) (Fig. 4c, d). We introduced the term switching efficiency (equation (3), Methods), given by the difference in the populations of the holo conformation at two ligand concentrations. Although the cellular concentration of adenine in *Escherichia coli* has been reported to be in the range of 1.5 μM[25], the differences in ligand concentration at which regulation occurs are unknown. We therefore considered a change in ligand concentration

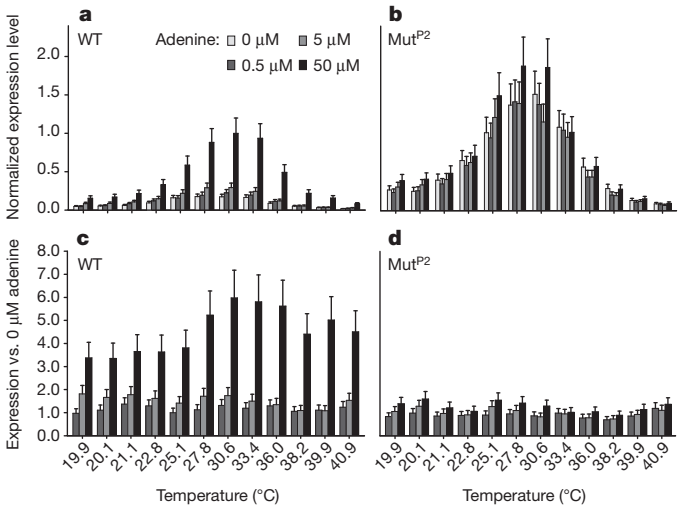

Figure 3 | Adenine-dependent expression regulation is only detected for the wild-type riboswitch. Transcription–translation-coupled *in vitro* luciferase assays at adenine concentrations from 0 to 50 μM between 20 °C and 41 °C. **a**, **b**, Expression levels of wild type (**a**) and Mut^{P2} (**b**), normalized against the highest wild-type raw value (30.6 °C, 50 μM). The overall expression level of Mut^{P2} showed a twofold increase compared to wild type. Error bars represent the standard deviation of three independent measurements. **c**, **d**, Expression levels of wild type (**c**) and Mut^{P2} (**d**), normalized against the respective values at 0 μM adenine. At 50 μM adenine, expression levels of wild type were increased over the entire temperature range by up to sixfold, whereas Mut^{P2} showed no adenine-dependent increase beyond experimental error, representing a constitutive on-state. Adenine independence was also observed in the expression of a luciferase control plasmid lacking either upstream riboswitch (Supplementary Fig. 10). Error bars are calculated by error propagation from the standard deviation of three independent measurements shown in **a** and **b**.

©2013 Macmillan Publishers Limited. All rights reserved

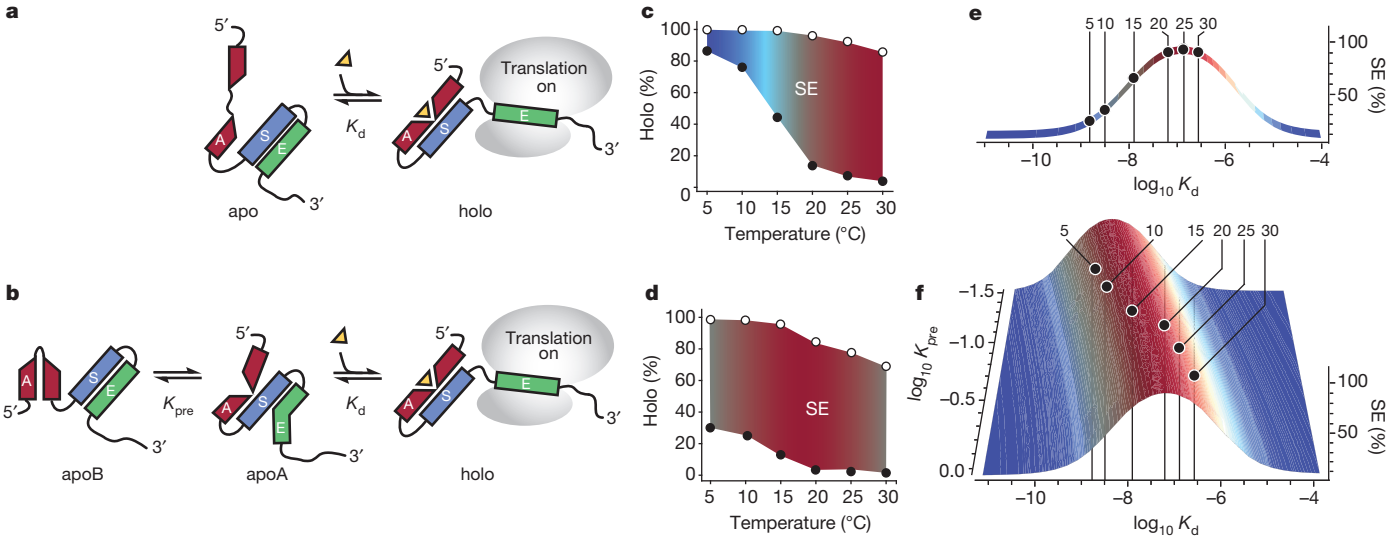

Figure 4 | Ligand-dependent conformational equilibria and simulation of the switching efficiency. **a**, **b**, Schematic picture of the two-state model (**a**) and the three-state model proposed here (**b**) for riboswitch regulation. Structural changes of aptamer (A), switching sequence (S) and effector sequence (E) are shown. **c**, Simulation of the temperature-dependent changes of the holo population for two adenine concentrations (0.01 μM (filled circles) and 1.5 μM (open circles)) at cellular mRNA concentrations of 1 nM for a two-state model. The switching efficiency (SE) is the area between the two holo populations for each temperature. **d**, Simulation of the temperature-dependent changes of the holo population for two adenine concentrations (0.01 μM (filled circles) and 1.5 μM (open circles)) at cellular mRNA concentrations of 1 nM for a three-state model. The switching efficiency is the area between the two holo populations for each temperature. **e**, Simulation of the switching efficiency for riboswitches regulating gene expression with a two-state mechanism. The dependence of the switching efficiency on temperature without pre-equilibrium is shown. In the simulations, the adenine concentration changes from 0.01 to 1.5 μM and the RNA concentration is 1 nM. **f**, Simulation of the switching efficiency for riboswitches regulating gene expression with a three-state mechanism. Simulations were performed assuming the experimentally determined K_d and K_{pre} and changes in adenine concentration from 0.01 to 1.5 μM at a RNA concentration of 1 nM. The switching efficiency is constant over the given temperature range. All simulations are based on data measured at 2 mM Mg^{2+}.

from 0.01 to 1.5 μM for the two-state and three-state mechanism. The temperature-dependent changes of K_d significantly affected the switching efficiency for a two-state riboswitch: we found an increase in switching efficiency from 14% to 85% for a change in temperature from 5 to 30 °C (Fig. 4c, e). Owing to the pre-equilibrium in the wild type, the riboswitch was able to maintain a switching efficiency between 67% and 83% in the same temperature range (Fig. 4d, f). At low temperatures, the affinity of the riboswitch to adenine was high ($\log K_d = -8.5$) and at the same time, the pre-equilibrium was shifted towards the inactive apoB conformation. At higher temperatures, a potentially lower switching efficiency due to lower affinity ($\log K_d = -6.6$) was counteracted by a shift in the pre-equilibrium towards a higher population of apoA.

In conclusion, we found that three conformations, linked by two equilibria, were functionally relevant for the translational adenine-sensing riboswitch. This three-state behaviour (Fig. 4b) maintained constant switching efficiency for a larger variation in temperature and a tighter dependence on ligand concentration than a two-state riboswitch (Fig. 4a) could achieve. The temperature-responsive mechanism was clearly distinct from typical zipper-like thermometers[26,27], and might have an important role in *Vibrio* biology when the pathogen is transferred to humans from its marine habitat. In fact, genes in *V. vulnificus* encoded on chromosome II have been suggested to adapt to environmental conditions[28]. The findings, however, have more general significance. By characterizing the sequence requirements for a three-state switch, we provided important information for synthetic biology applications of riboswitches. Furthermore, the three-state mechanism, also evidenced in conformational selection processes during ligand binding for a second riboswitch[29], is applicable in biomolecular assemblies in general. The ability to sense variations in temperature and ligand concentration simultaneously leads us to propose the term 'riboswitch-thermostat' for this new function in regulatory RNA elements.

METHODS SUMMARY

The unlabelled and ^{15}N-labelled RNA constructs were synthesized using T7 polymerase. All NMR experiments were performed in NMR buffer (25 mM potassium phosphate, 50 mM potassium chloride, pH 6.2) containing 10% D_2O on Bruker spectrometers and analysed with Topspin. To determine k_{AB} and k_{BA}, two-dimensional ^1H–^{15}N heteronuclear exchange experiments were recorded on the full-length RNA without adenine. To record kinetics of the tertiary complex formation, NMR real-time kinetic experiments of the wild-type and Mut^{P2} RNA were conducted using a rapid sample mixing device. Binding affinities of adenine to wild-type full-length RNA were determined by ITC on a microcalorimeter (Microcal) in NMR buffer at different Mg^{2+} concentrations and temperatures. Stopped-flow kinetics were measured on an Applied Photophysics π*-180 fluorescence spectrometer. The experiments were measured under pseudo-first order conditions in NMR buffer containing 2 mM Mg^{2+}. The fluorescent analogue of adenine, 2-aminopurine, was used. The inverted apparent rate constant $1/\tau$ was plotted against the RNA concentration to determine k_{on}, k_{off} and K_d values using equation (1)

$$\frac{1}{\tau} = k_{on}[\mathrm{RNA_0}] + k_{off} \quad (1)$$

Circular dichroism melting curves were recorded on a J-810 CD spectrometer (Jasco) in NMR buffer without Mg^{2+}. Luciferase *in vitro* expression assays were performed on a gradient thermocycler at different temperatures and at four different adenine concentrations using DNA templates with wild-type, Mut^{P2} or no riboswitch cloned upstream of the firefly luciferase start codon. Expression levels were quantified on a microplate luminometer.

Theoretical simulations were performed using scripts written in the program Mathematica. The population of the holo conformation was calculated using equation (2)

$$P[\mathrm{holo}] = \frac{100}{2[\mathrm{RNA_0}]K_{pre}}\left(K_d + K_dK_{pre} + K_{pre}[L_0] + K_{pre}[\mathrm{RNA_0}] - \sqrt{-4K_{pre}{}^2[L_0][\mathrm{RNA_0}] + \left(K_d + K_dK_{pre} + K_{pre}[L_0] + K_{pre}[\mathrm{RNA_0}]\right)^2}\right) \quad (2)$$

©2013 Macmillan Publishers Limited. All rights reserved

Full Methods and any associated references are available in the online version of the paper.

Received 25 April; accepted 12 June 2013.
Published online 10 July 2013.

1. Mironov, A. S. *et al.* Sensing small molecules by nascent RNA: a mechanism to control transcription in bacteria. *Cell* **111,** 747–756 (2002).
2. Winkler, W., Nahvi, A. & Breaker, R. R. Thiamine derivatives bind messenger RNAs directly to regulate bacterial gene expression. *Nature* **419,** 952–956 (2002).
3. Nahvi, A. *et al.* Genetic control by a metabolite binding mRNA. *Chem. Biol.* **9,** 1043–1049 (2002).
4. Garst, A. D., Edwards, A. L. & Batey, R. T. Riboswitches: structures and mechanisms. *Cold Spring Harb. Perspect. Biol.* **3,** a003533 (2011).
5. Winkler, W. C. & Breaker, R. R. Genetic control by metabolite-binding riboswitches. *Chembiochem* **4,** 1024–1032 (2003).
6. Mandal, M. & Breaker, R. R. Adenine riboswitches and gene activation by disruption of a transcription terminator. *Nature Struct. Mol. Biol.* **11,** 29–35 (2004).
7. Wickiser, J. K., Cheah, M. T., Breaker, R. R. & Crothers, D. M. The kinetics of ligand binding by an adenine-sensing riboswitch. *Biochemistry* **44,** 13404–13414 (2005).
8. Lemay, J. F. & Lafontaine, D. A. Core requirements of the adenine riboswitch aptamer for ligand binding. *RNA* **13,** 339–350 (2007).
9. Greenleaf, W. J., Frieda, K. L., Foster, D. A., Woodside, M. T. & Block, S. M. Direct observation of hierarchical folding in single riboswitch aptamers. *Science* **319,** 630–633 (2008).
10. Lemay, J. F., Penedo, J. C., Tremblay, R., Lilley, D. M. & Lafontaine, D. A. Folding of the adenine riboswitch. *Chem. Biol.* **13,** 857–868 (2006).
11. Noeske, J. *et al.* An intermolecular base triple as the basis of ligand specificity and affinity in the guanine- and adenine-sensing riboswitch RNAs. *Proc. Natl Acad. Sci. USA* **102,** 1372–1377 (2005).
12. Lemay, J. F. *et al.* Comparative study between transcriptionally- and translationally-acting adenine riboswitches reveals key differences in riboswitch regulatory mechanisms. *PLoS Genet.* **7,** e1001278 (2011).
13. Neupane, K., Yu, H., Foster, D. A., Wang, F. & Woodside, M. T. Single-molecule force spectroscopy of the add adenine riboswitch relates folding to regulatory mechanism. *Nucleic Acids Res.* **39,** 7677–7687 (2011).
14. Rieder, R., Lang, K., Graber, D. & Micura, R. Ligand-induced folding of the adenosine deaminase A-riboswitch and implications on riboswitch translational control. *Chembiochem* **8,** 896–902 (2007).
15. Serganov, A. *et al.* Structural basis for discriminative regulation of gene expression by adenine- and guanine-sensing mRNAs. *Chem. Biol.* **11,** 1729–1741 (2004).
16. Lee, M. K., Gal, M., Frydman, L. & Varani, G. Real-time multidimensional NMR follows RNA folding with second resolution. *Proc. Natl Acad. Sci. USA* **107,** 9192–9197 (2010).
17. Wang, J. *et al.* A method for helical RNA global structure determination in solution using small-angle X-ray scattering and NMR measurements. *J. Mol. Biol.* **393,** 717–734 (2009).
18. Dixon, N. *et al.* Reengineering orthogonally selective riboswitches. *Proc. Natl Acad. Sci. USA* **107,** 2830–2835 (2010).
19. Farrow, N. A., Zhang, O., Forman-Kay, J. D. & Kay, L. E. A heteronuclear correlation experiment for simultaneous determination of ^{15}N longitudinal decay and chemical exchange rates of systems in slow equilibrium. *J. Biomol. NMR* **4,** 727–734 (1994).
20. Stoddard, C. D. *et al.* Nucleotides adjacent to the ligand-binding pocket are linked to activity tuning in the purine riboswitch. *J. Mol. Biol.* **425,** 1596–1611 (2013).
21. Buck, J., Furtig, B., Noeske, J., Wohnert, J. & Schwalbe, H. Time-resolved NMR methods resolving ligand-induced RNA folding at atomic resolution. *Proc. Natl Acad. Sci. USA* **104,** 15699–15704 (2007).
22. Mok, K. H. *et al.* Rapid sample-mixing technique for transient NMR and photo-CIDNP spectroscopy: Applications to real-time protein folding. *J. Am. Chem. Soc.* **125,** 12484–12492 (2003).
23. Li, Y. C., Li, Y. M., Zhang, H. & Chen, Y. MicroRNA-mediated positive feedback loop and optimized bistable switch in a cancer network involving miR-17–92. *PLoS ONE* **6,** e18954 (2011).
24. Selinger, D. W. *et al.* RNA expression analysis using a 30 base pair resolution *Escherichia coli* genome array. *Nature Biotechnol.* **18,** 1262–1268 (2000).
25. Bennett, B. D. *et al.* Absolute metabolite concentrations and implied enzyme active site occupancy in *Escherichia coli. Nature Chem. Biol.* **5,** 593–599 (2009).
26. Rinnenthal, J., Klinkert, B., Narberhaus, F. & Schwalbe, H. Direct observation of the temperature-induced melting process of the *Salmonella* fourU RNA thermometer at base-pair resolution. *Nucleic Acids Res.* **38,** 3834–3847 (2010).
27. Kortmann, J. & Narberhaus, F. Bacterial RNA thermometers: molecular zippers and switches. *Nature Rev. Microbiol.* **10,** 255–265 (2012).
28. Xu, Q., Dziejman, M. & Mekalanos, J. J. Determination of the transcriptome of *Vibrio cholerae* during intraintestinal growth and midexponential phase *in vitro. Proc. Natl Acad. Sci. USA* **100,** 1286–1291 (2003).
29. Wilson, R. C. *et al.* Tuning riboswitch regulation through conformational selection. *J. Mol. Biol.* **405,** 926–938 (2011).

Supplementary Information is available in the online version of the paper.

Acknowledgements We thank E. Stirnal, H. Keller and C. Richter for technical support. We thank F. Narberhaus, J. Wöhnert, J. Wachtveitl, J. Soppa, E. Schleiff, A. Heckel, M. Hengesbach and C. Griesinger for stimulating discussions. This work was funded by the German funding agency (DFG) in Collaborative Research Center 902.

Author Contributions A.R., S.N., K.S., F.B. and B.F. conducted experiments. All authors contributed to the analysis of the data and the writing of the manuscript.

Author Information Reprints and permissions information is available at www.nature.com/reprints. The authors declare no competing financial interests. Readers are welcome to comment on the online version of the paper. Correspondence and requests for materials should be addressed to H.S. (schwalbe@nmr.uni-frankfurt.de) or B.F. (fuertig@nmr.uni-frankfurt.de).

©2013 Macmillan Publishers Limited. All rights reserved

METHODS

RNA preparation. The unlabelled and ^{15}N-labelled RNA constructs were synthesized by *in vitro* transcription using T7 polymerase and purified as described[30]. All RNAs were folded by thermal denaturation of the RNA at high concentration (0.2–0.5 mM), diluted to 0.05 mM, and rapidly cooled on ice. Folding into a homogenous conformation was verified by native PAGE. Samples were exchanged into NMR buffer (25 mM potassium phosphate, 50 mM potassium chloride, pH 6.2). A 5′-hammerhead ribozyme[31] was used for the transcription of wild-type and Mut^{P2} RNAs.

Synthesis of labelled adenine. The ^{13}C,^{15}N-labelled adenine was synthesized and analysed as described previously[11]. The concentration of the labelled adenine was estimated using ultraviolet absorbance at 261 nm, using $\varepsilon^{261\mathrm{nm}} = 13.400\ \mathrm{mol}^{-1}\ \mathrm{cm}^{-1}$(ref. 32).

NMR spectroscopy. NMR experiments were conducted on Bruker spectrometers (AV600-AV950). Processing and analysis of the data were performed using the software programs topspin 1.3-3.1 (Bruker BioSpin, Rheinstetten) and Sparky 3.114 (T. D. Goddard & D. G. Kneller, University of California, San Francisco). Samples contained 90% H_2O and 10% D_2O.

Assignment of secondary and tertiary structure elements within the apo and holo states of the RNA were based on the chemical shift assignments of imino proton resonances (Fig. 1). These resonances are reporters for the interaction between adjacent base pairs, and were assigned using NOESY (nuclear Overhauser enhancement spectroscopy) and HSQC experiments, and by comparing experiments of full-length RNAs with fragment structural reference modules (Supplementary Figs 2–4 and Supplementary Tables 1 and 2).

$^{15}N_{ZZ}$-exchange. Two-dimensional ^{1}H–^{15}N heteronuclear exchange experiments[19] were recorded to determine the rate of interconversion between the apo states. For the ligand-free wild-type full-length RNA, nucleotides G43 and G44 yielded detectable imino proton signals in both folds (Supplementary Fig. 6a, b). Owing to spectral overlap, only the time dependence of peak heights of the diagonal and cross peaks of G44 (mixing times: 0–0.8 s) were quantified (Fig. 1d and Supplementary Fig. 6). Data points were fitted with Mathematica (Wolfram Research) to extract the chemical exchange rates k_{AB} and k_{BA}. The experiments were performed on an AV700 spectrometer with 0 and 2 mM Mg^{2+} at 25 °C, and with 2 mM Mg^{2+} at 30 °C (Supplementary Fig. 6c).

Real-time NMR kinetics. NMR real-time kinetic experiments of the wild-type and Mut^{P2} RNA were conducted on an AV800 spectrometer at 20 °C with 2 mM Mg^{2+}. The reaction was initiated inside a shigemi-tube using a rapid sample mixing device[22]. Three-hundred microlitres of 0.3 mM RNA was mixed with 40 µl of 5 mM adenine solution to prepare an [RNA]:[ligand] ratio of 1:2. For the wild-type construct, a selectively ^{15}N-uridine-labelled RNA in combination with ^{15}N-filtered/edited experiments[21,33] was used. For the Mut^{P2} construct, a fully labelled RNA was used. The experiments were recorded as a pseudo-2D dataset[34]. The overall apparent wild-type and MutP2 k_F rate constants for folding of the complexes were determined by calculating the sum of all normalized imino proton signal integrals that showed time-dependent changes and were well resolved. The obtained kinetic traces were fitted with a mono-exponential function.

ITC RNA-binding assays. The binding affinities between adenine and full-length wild-type RNA were measured using a microcalorimeter (Microcal). The RNA (40 µM) and adenine (100 µM) were dissolved in NMR buffer containing 2 mM Mg^{2+}. Measurements were performed at 10 °C and 30 °C. K_d (equilibrium binding constant) values were calculated by fitting the raw ITC data with nonlinear least-squares analysis (Fig. 1d, e).

Stopped-flow kinetics. Stopped-flow kinetics were measured on an Applied Photophysics π*-180 fluorescence spectrometer. A fluorescent analogue of adenine, 2-aminopurine, binds to the adenine-sensing riboswitch aptamer, similar to the cognate ligand adenine[6,10,15]. RNA and 2-aminopurine were dissolved in NMR buffer containing 2 mM $MgCl_2$. The 2-aminopurine concentration was calculated using ultraviolet absorbance at 305 nm[32]. We performed the stopped-flow measurements and analysis as previously described[7]. The RNA concentration was varied from 100 nM to 1 mM in excess over 2-aminopurine (50 nM). Rate constants were determined at 10, 15, 20, 25 and 30 °C for the wild-type RNA, and at 15, 20 and 25 °C for Mut^{P2} RNA. The fluorescence decay was fitted to a mono-exponential decay with three parameters (Supplementary Fig. 9). The resulting apparent rate constants used for analysis are averaged values of at least three independent measurements (Supplementary Table 3). Association (k_{on}) and dissociation (k_{off}) rate constants were determined by plotting the inverted apparent rate constant $1/\tau$ versus the RNA concentration ([RNA_0]) using equation (1) (Supplementary Table 4):

$$\frac{1}{\tau} = k_{on}[RNA_0] + k_{off} \quad (1)$$

Circular dichroism melting. Circular dichroism melting curves were recorded on a J-810 CD spectrometer (Jasco) using a 1-mm quartz cuvette, with 250 µl volume at a wavelength of 264 nm. The RNA concentration was 5 µM in NMR buffer. Spectra were recorded with 10 µM adenine and without Mg^{2+}. Circular dichroism melting curves were analysed according to the literature[35,36].

Luciferase *in vitro* expression assays. DNA constructs of wild-type and Mut^{P2} were designed as follows. The triplet A120-U121-G122 downstream of the ribosome-binding site of the adenine riboswitch constituted the start codon of a firefly luciferase reporter gene. The constructs were cloned into the plasmid pET23(+), which carries no intrinsic ribosome-binding site. For negative control experiments, a T7 luciferase control plasmid (Promega) was used (Supplementary Fig. 11).

For the assay, 15 µg of template DNA were added to a total volume of 200 µl of a transcription–translation-coupled *E. coli*-based *in vitro* expression system (RTS 100 *E. coli* HY, 5 PRIME GmbH), supplemented with 250 U of RNase inhibitor (RiboLock, Thermo Scientific). One microlitre of adenine stock solutions of 25 mM, 2.5 mM and 250 µM, respectively, were added to 50-µl aliquots of the reaction mix, which were then further divided into 4-µl aliquots and incubated on a gradient thermocycler (Eppendorf AG) for 1 h with a temperature gradient of 20–41 °C.

Samples (2.5 µl) of each aliquot were then added to 50 µl of SteadyGlo luciferase substrate solution (Promega) on a microtitre plate. After 5 min incubation at room temperature, bioluminescence was quantified using a Veritas Microplate Luminometer (Turner BioSystems). All experiments were performed in triplicates, with a total Mg^{2+} concentration of 12 mM.

Simulations. Simulation of the population of the holo RNA conformation (P[holo]) and switching efficiency (SE) were performed using scripts written in the program Mathematica using equations (2) and (3):

$$P[\mathrm{holo}] = \frac{100}{2[\mathrm{RNA}_0]K_{pre}}\left(K_d + K_d K_{pre} + K_{pre}[L_0] + K_{pre}[\mathrm{RNA}_0] - \sqrt{-4K_{pre}{}^2[L_0][\mathrm{RNA}_0] + \left(K_d + K_d K_{pre} + K_{pre}[L_0] + K_{pre}[\mathrm{RNA}_0]\right)^2}\right) \quad (2)$$

$$\mathrm{SE}(L_{0,1}, L_{0,2}, \mathrm{RNA}_0) = P[\mathrm{holo}](L_{0,1}, \mathrm{RNA}_0) - P[\mathrm{holo}](L_{0,2}, \mathrm{RNA}_0) \quad (3)$$

Derivation of the equations is detailed in Supplementary Information.

30. Stoldt, M., Wohnert, J., Ohlenschlager, O., Gorlach, M. & Brown, L. R. The NMR structure of the 5S rRNA E-domain–protein L25 complex shows preformed and induced recognition. *EMBO J.* **18,** 6508–6521 (1999).
31. Birikh, K. R., Heaton, P. A. & Eckstein, F. The structure, function and application of the hammerhead ribozyme. *Eur. J. Biochem.* **245,** 1–16 (1997).
32. Fasman, G. D. *Handbook of Biochemistry and Molecular Biology, Nucleic Acids* 3rd edn, Vol. 1, 65–215 (CRC Press, 1975).
33. Piotto, M., Saudek, V. & Sklenar, V. Gradient-tailored excitation for single-quantum NMR spectroscopy of aqueous solutions. *J. Biomolec. NMR* **2,** 661–665 (1992).
34. Wacker, A., Buck, J., Richter, C., Schwalbe, H. & Wohnert, J. Mechanisms for differentiation between cognate and near-cognate ligands by purine riboswitches. *RNA Biol.* **9,** 672–680 (2012).
35. Marky, L. A. & Breslauer, K. J. Calculating thermodynamic data for transitions of any molecularity from equilibrium melting curves. *Biopolymers* **26,** 1601–1620 (1987).
36. Mergny, J. L. & Lacroix, L. Analysis of thermal melting curves. *Oligonucleotides* **13,** 515–537 (2003).

©2013 Macmillan Publishers Limited. All rights reserved